Anal. Chem. **2004,** *76,* 2719−2724

Mechanistic Investigation of Nanoparticle Motion in Pulsed Voltage Miniaturized Electrical Field Flow Fractionation Device by in Situ Fluorescence Imaging

Alex Ieng Kin Lao,[†] Yi-Kuen Lee,[‡] and I-Ming Hsing*,[†]

Department of Chemical Engineering and Department of Mechanical Engineering, Hong Kong University of Science and Technology, Hong Kong SAR

In our previous study, we reported a miniaturized electrical field flow fractionation device (μ-EFFF) that used a pulsed voltage (PV) to increase the effective electric field and, hence, improved the separation performance. In this work, we developed two μ-EFFFs with planar or segmented electrode design and investigated the particle movement in the flow channels under a PV. Numerical simulation was used to understand the electric field distribution in the μ-EFFFs. When the calculations for the μ-EFFF with a segmented electrode (segmented μ-EFFF) and the μ-EFFF with planar electrodes (planar μ-EFFF) are compared, a stronger electric field at the top electrode segments is found in the segmented μ-EFFF, with the strongest field at the edges of the electrode segments. Nanoparticle motion in both devices was in situ visualized by using a fluorescence microscope equipped with a CCD-camera. Results reveal that electrophoresis governs the nanoparticle movement in the planar μ-EFFF and dielectrophoresis dominates the movement in the segmented μ-EFFF. Two models are postulated to explain the experimental observations of the nanoparticle movement. The mechanistic understanding of controlling nanoparticle motion in a miniaturized environment will help the design and application of μ-EFFF for the separation of charged biomolecules (proteins and DNAs).

Electrical field flow fractionation (EFFF) is a powerful analytical technique that relies on an electric field perpendicular to the direction of separation to fractionate colloids with respect to the particle size and electrophoretic mobility. It is gaining significance for the micro total analysis system (μ-TAS) because of its capability to separate a broad size range of biomolecules and particles and its feasibility for miniaturization.

EFFF was first described in 1972 as a technique for separating proteins.[1] Little progress was made at first due to the reported poor separation performance until an improved design was introduced in 1993, which used the electrodes as the channel walls for latex particles separation.[2] The effects of deterministic parameters, such as carrier ionic strength, carrier flow rate, and the amount of injected sample, on the separation performance were investigated by using the improved EFFF device;[3,4] however, the separation performance was limited by a weak effective electric field across the flow channel.

In 1997, the first miniaturized EFFF device (μ-EFFF) was introduced for separation of latex particles.[5] It gained inherent advantages from miniaturization, such as a stronger electric field and increased resolution;[6] however, one major technical obstacle in using the μ-EFFF to separate microsamples was the weak effective electric field caused by polarization layers on electrode surfaces.[5,7] In our previous study,[8] we used a μ-EFFF operated with pulsed voltage (PV) to increase the effective electric field and reported an improved separation performance. Other researchers reported a dielectrophoretic field flow fractionation (DEP-FFF) device with an interdigitated electrode design that operated with an AC excitation to successfully separate particles and cells with a diameter of 6 μm or larger by utilizing the effects of negative dielectrophoresis and sedimentation.[9−11]

A model for EFFF under a constant voltage was developed by under the assumption that the balance between diffusion and electrophoresis led to a defined lateral position of the particle.[12] A generalized model for all types of field flow fractionation (FFF) using a cyclical field was postulated in 1986.[13] The particles in

* Corresponding author. Phone: 852-23587131. Fax: 852-23580054. E-mail: kehsing@ust.hk.

[†] Department of Chemical Engineering.

[‡] Department of Mechanical Engineering.

(1) Caldwell, K. D.; Kesner, L. F.; Myer, M. N.; Giddings, J. C. *Science* **1972**, *176*, 296−298.

(2) Caldwell, K. D.; Gao, Y. S. *Anal. Chem.* **1993**, *65*, 1764−1772.

(3) Palker, S. A.; Schure, M. R. *Anal. Chem.* **1997**, *69*, 3223−3229.

(4) Palker, S. A.; Schure, M. R. *Anal. Chem.* **1997**, *69*, 3230−3238.

(5) Gale, B. K.; Caldwell, K. D.; Frazier, A. B. *IEEE Micro Electro Mech. Syst.* **1997**, 119−214.

(6) Gale, B. K.; Caldwell, K. D.; Frazier, A. B. *Anal. Chem.* **2001**, *73*, 2345−2352.

(7) Gale, B. K.; Caldwell, K. D.; Frazier, A. B. *Anal. Chem.* **2002**, *74*, 1024−1030.

(8) Lao, A. I. K.; Trau, D.; Hsing, I. M. *Anal. Chem.* **2002**, *74*, 5364−5369.

(9) Huang, Y.; Wang, X. B.; Becker, F. F.; Gascoyne, P. R. C. *Biophys. J.* **1997**, *73*, 1118−1129.

(10) Wang, X. B.; Vykoukal, J.; Becker, F. F. B.; Gascoyne, P. R. C. *Biophys. J.* **1998**, *74*, 2689−2701.

(11) Wang, X. B.; Yang, J.; Huang, Y.; Vykoukal, J.; Bekcer, F. F.; Gascoyne, P. R. C. *Anal. Chem.* **2000**, *72*, 832−839.

(12) Schimpf, M. E.; Caldwell, K.; Giddings, J. C. *Field Flow Fractionation Handbook*; Wiley-Interscience: New York, 2000.

(13) Giddings, J. C. *Anal. Chem.* **1986**, *58*, 2052−2056.

10.1021/ac035429y CCC: $27.50
Published on Web 04/03/2004

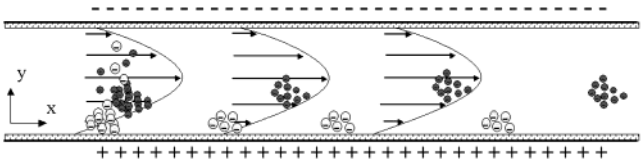

Figure 1. Schematic illustration of an EFFF device operated with a constant voltage. Particles with different electrophoretic mobilities are levitated by the electric field to different lamina of the hydrodynamic flow with a parabolic flow profile and are carried through the flow channel with different velocities.

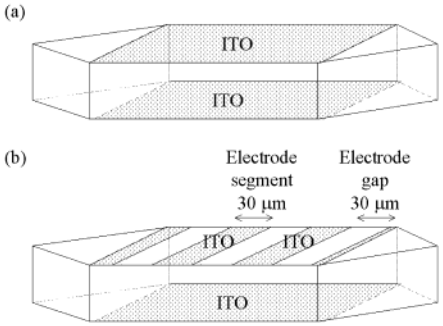

Figure 2. Structure of the μ-EFFF with (a) a pair of planar electrodes (planar μ-EFFF) and (b) a bottom-planar electrode and a top-segmented electrode with alternating 30-μm-wide electrode segments and electrode gaps (segmented μ-EFFF).

the flow channel were assumed to be affected by a field-derived force only, whereas forces from Brownian motion and diffusion were neglected. Their movement was assumed to be coherent with the cyclical field. Thus, the lateral migration rate depended solely on the transport coefficient of the particles.

In this study, we demonstrate two μ-EFFFs with different electrode designs, one of which has a pair of planar electrodes (planar μ-EFFF) and the other has a bottom-planar electrode and a top-segmented electrode (segmented μ-EFFF). The segmented electrode was produced by alternating conductive material (electrode segment) and insulating material (electrode gap) with equal widths of 30 μm. Both devices were fabricated on indium tin oxide (ITO)-coated glass. Electric field distributions for both μ-EFFFs were investigated numerically under a constant voltage. Particle motion in the flow channels under a PV was in situ visualized by an inverted fluorescence microscope equipped with a CCD camera. Mechanistic models of these two μ-EFFFs were postulated.

THEORY

FFF relies on an external field perpendicular to the pressure driven flow with a parabolic flow profile.[12] Particles injected into a FFF device interact with the external field. Depending on the strength of their interaction, the particles are positioned in a particular lamina of the pressure driven flow with a specific distance $y(t)$ from the accumulation wall of the device. Due to the parabolic flow profile of the pressure driven flow, particles located at different lamina travel with different velocities and, thus, elute the system at different times. The momentary particle velocity $v_x(y, t)$ at a distance $y(t)$ from the accumulation wall can be written as

$$v_x(y, t) = 6\langle v\rangle\left(\frac{y(t)}{w} - \frac{y(t)^2}{w^2}\right) \qquad (1)$$

where $\langle v\rangle$ is the average fluid velocity and w is the channel thickness.

The overall mean velocity of the particle, V, in the device is determined by the axial velocity, v_x, and can be expressed as

$$V = \frac{1}{\tau}\int_{t=0}^{\tau} v_x(y, t)\, \mathrm{d}t \qquad (2)$$

where τ is the elution time of the particle.

In a typical EFFF device (Figure 1), a stable electric field, $E(y)$, is generated by applying a constant voltage (CV) between two planar electrodes. Charged particles inside the system are driven by electrophoresis toward the electrode of the opposite polarity. This electrophoretic force can be written as a product of the particle charge, q, and the electric field strength. As the particles accumulate close to the electrode, the flux of the particles is opposed by diffusion. Thus, the distance of a particle, $y(t)$, to the electrode is determined by these two opposing transport processes. At equilibrium, a balance between diffusion and electrophoresis leads to a defined lateral position of the particle, y, to the electrode. Consequently, the overall mean velocity of the particle, V, is commonly assumed to be a constant in the CV mode of operation.

However, while applying a pulsed voltage (PV) to the device, particles do not have sufficient time to reach equilibrium. The distance of the particle, $y(t)$, to the electrode is predominantly determined by electrophoresis. A temporary equilibrium may result if the time to achieve a steady state is shorter than one-half the time interval of the PV. In both cases, the distance of the particle, $y(t)$, from the electrode varies coherently with the polarity change of the PV. The overall mean particle velocity, V, is therefore not a constant and should be expressed in the integral form of eq 2. Due to the periodic pattern of the PV, the elution time τ in eq 2 can be replaced by the time interval of the PV τ_c.

Dielectrophoresis (DEP) is the translational motion of a particle as a result of polarization induced by a nonuniform electric field.[14] The particle is driven toward (positive DEP) or away from (negative DEP) the strong-field region depending on the frequency-dependent complex dielectric permittivity of the particle ϵ_p^* and its suspending medium ϵ_m^*. The dielectrophoretic force F_{DEP} acting on a particle with radius r at distance $y(t)$ from the segmented electrode of the EFFF device with a segmented electrode design, such as Figure 2b, can be written as[14]

$$F_{\mathrm{DEP}} = 2\pi r^3 \epsilon_0 \epsilon_{\mathrm{m}} \mathrm{Re}\left[\frac{\epsilon_p^* - \epsilon_m^*}{\epsilon_p^* + 2\epsilon_m^*}\right]\nabla|E(x, y)|^2 \qquad (3)$$

where ϵ_0 is the permittivity of free space (8.854×10^{-12} F m^{-1}) and $|E(x, y)|$ is the RMS magnitude of the local electric field.

The local electric field is used due to the nonuniform distribution of the electric field in the EFFF device. The real component of the Clausius−Mossotti factor $\mathrm{Re}[(\epsilon_p^* - \epsilon_m^*)/(\epsilon_p^* + 2\epsilon_m^*)]$

(14) Pohl, H. A. *Dielectrophoresis*; Cambridge University Press: Cambridge, 1978.

denotes the direction of DEP and has a theoretical value ranging from −0.5 to 1.0. The dielectrophoretic force depends on the square of the magnitude of electric field strength as compared to electrophoresis, which is proportional to the electric field strength. The DEP force is also sensitive to the size of particles (up to the power 3 of the particle radius), as illustrated in eq 3.

The sedimentational force F_{SED} acting on a particle with radius r can be expressed as

$$F_{SED} = \frac{4}{3}\pi r^3(\rho_p - \rho_m)g \quad (4)$$

where ρ_p is the particle density, ρ_m is its suspending medium density, and g is the acceleration of gravity (9.807 m s^{-2}).

Together with the diffusive force, these forces determine the distance of the particle, $y(t)$, to the electrode. The overall mean particle velocity, V, in the EFFF device with a segmented electrode design can be expressed as in eq 2. An integral form is used because of the nonuniform distribution of the electric field, which causes a spatially nonuniform DEP. This will be explained in the Results and Discussion.

EXPERIMENTAL METHODS

Materials. *Sample.* Fluorescent carboxylated surface-modified polystyrene (PS) particles of 0.45-μm diameter (Sigma Chemical, St. Louis, MO) were used as a sample.

Carrier. Pure deionized water (Milli-Q system, Millipore, Bedford, MA) was used as a carrier solution. Prior to its use, it was filtered through a 0.44-μm filter and purged with nitrogen gas to remove the dissolved oxygen in order to minimize generation of bubbles and maintain a constant conductivity of the carrier solution.

μ-EFFFs. Two designs of μ-EFFF were fabricated for this study. One device has a top-planar electrode (Figure 2a, hereafter termed as planar μ-EFFF) similar to that described in an earlier publication,[8] and the other device has a top-segmented electrode (Figure 2b, hereafter termed as segmented μ-EFFF) produced by alternating 30-μm conductive material (electrode segment) and insulating material (electrode gap). The bottom electrodes of both μ-EFFFs were planar. The heights and volumes of the flow channels were 20 μm and 20 μL, respectively, for both devices.

The fabrication procedures of the μ-EFFFs were identical to the previous study,[8] except for a higher rotation speed at the spin-coating step to deposit the Su-8 photo resist (Microchem, Newton, Massachusetts) material.

Simulation. Commercial computational fluid mechanics software (CFD-ACE, CFD Research Corporation, Huntsville, AL) was used to simulate the electric field distribution in both μ-EFFFs. The Laplace equation was used as the governing equation. A constant voltage of 1.75 V was applied to the top electrode of the planar μ-EFFF. For the segmented μ-EFFF, the voltage was only applied to the electrode segments. The voltage on the bottom electrodes for both devices was set to 0 V.

Instrumentation. The μ-EFFF setup (Figure 3) was similar to that reported earlier in ref 8. PV was applied on the μ-EFFF by either a potentiostat (PGSTAT30, Autolab, Eco Chemie B.V.) or a function generator (HP 33120A, Hewlett-Packard, Santa Clara, CA). Particle motion in the μ-EFFF was in situ visualized under an inverted fluorescence microscope (IX-70, Olympus, Japan) and recorded using a cooled CCD camera (QImaging Regita 1300C, Qimaging Inc., B.C., Canada) or an intensified CCD camera (ICCD-350F, Videoscope International, LTD, Dulles, Virginia). Data were acquired by a computer by using a LabVIEW (National Instruments, Austin, TX) program through an IEEE 1394 interface for the cooled CCD camera or by using Navis-Pro through a Navis-Pro capture card for the intensified CCD camera.

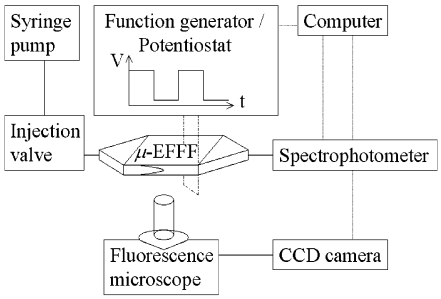

Figure 3. Schematic diagram of the experimental setup for the pulsed voltage (PV) μ-EFFF.

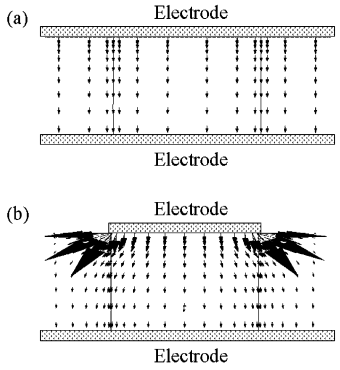

Figure 4. Two-dimensional plot of the electric field distribution across two electrodes for (a) planar μ-EFFF and (b) segmented μ-EFFF. The magnitude of the arrows corresponds to the electric field strength. A stronger electric field is observed at the top electrode segments of segmented μ-EFFF, with the strongest field at the edges.

Methods. A rectangular PV waveform of 10 Hz with amplitude of 1.7 V peak-to-peak (V_{pp}) and a duty cycle of 0.5 was applied on the electrodes of the μ-EFFF.

Particle motion was registered for both μ-EFFFs by applying a PV in the absence of a pressure driven flow. The effect of PV on the motion of a single nanoparticle was studied at a carrier flow rate of 10 μL h^{-1} for the segmented μ-EFFF. Motion of a nanoparticle in the segmented μ-EFFF was recorded at a carrier fluid flow rate of 5 μL h^{-1} after a PV had been applied to the device for a period of time.

RESULTS AND DISCUSSION

Electric Field Strength. The strength of the electric field in the two μ-EFFFs was simulated using the CFD-ACE software. Any probable double layers at the electrode-carrier interfaces were neglected in the computation. The electric field distribution across the two electrodes is illustrated in Figure 4a for the planar μ-EFFF and in Figure 4b for the segmented μ-EFFF. The size of an arrow is proportional to the strength of the electric field. A stronger electric field is observed for the top electrode segments of the segmented μ-EFFF, as compared to the top electrode of the planar

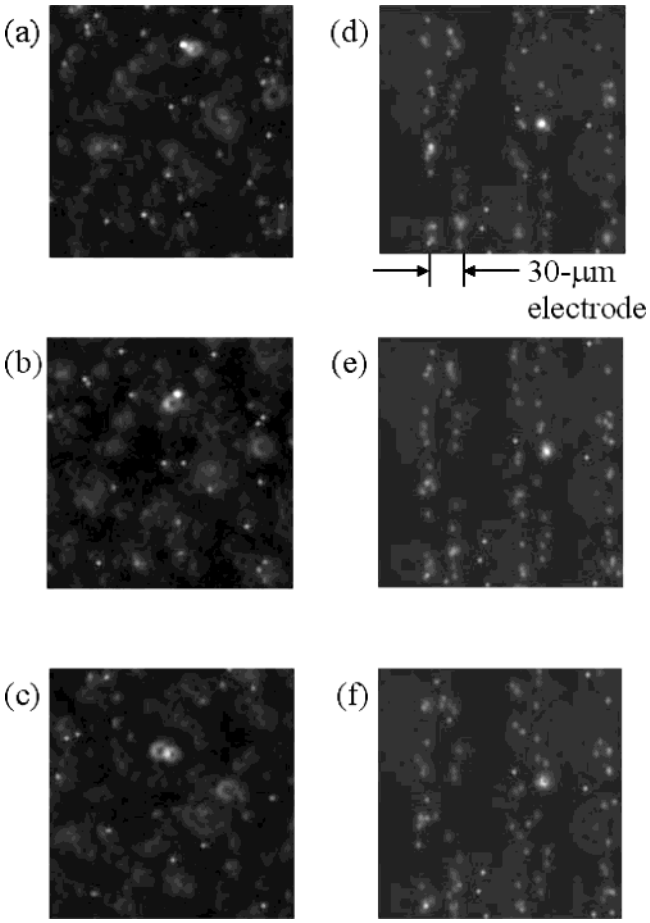

Figure 5. Sequential fluorescence photographs of PS nanoparticle motion for planar μ-EFFF at (a) 1, (b) 2, and (c) 3 and for segmented μ-EFFF at (d) 1, (e) 2, and (f) 3 s by applying a PV of 1.7 V peak-to-peak at 10 Hz. In the planar μ-EFFF, particles oscillate between two electrodes, and no obvious patterns can be seen; whereas in the segmented μ-EFFF, nanoparticles are clustered at the edges of the electrodes.

μ-EFFF. The strongest electric field is found at the edges of the electrode segments. Both μ-EFFFs have a similar electric field strength at the bottom electrodes.

Particle Motion. The effects of PV on particle motion in both μ-EFFFs were studied in the absence of a pressure driven flow. (See Supporting Information on videos, Figure 5a.avi for the planar μ-EFFF and Figure 5b.avi for the segmented μ-EFFF.) The particle motion was recorded in the absence of a PV for the first 5 s, then a PV of 10 Hz was applied for 5 s. Afterward, the PV was terminated. Sequential fluorescence photographs of the particle motion for the planar μ-EFFF are shown in Figure 5a−c and for the segmented μ-EFFF in Figure 5d−f.

Planar μ-EFFF. In the planar μ-EFFF, particles fluctuate randomly in the flow channel at the beginning due to the Brownian motion. Their fluctuation increases after a PV is applied because the particles experience electrophoresis and move up and down periodically between the two electrodes. The electrophoretic force and the sedimentational force acting on the particles are calculated as 2.75×10^{-15} N and 2.39×10^{-17} N, respectively. After the PV is stopped, the particles fluctuate randomly again.

Segmented μ-EFFF. In the segmented μ-EFFF, the particles also undergo Brownian motion in the absence of a PV, as in the

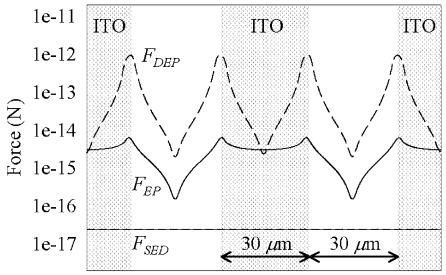

Figure 6. Force analysis diagram for the nanoparticles at 1 μm from the segmented electrode of segmented μ-EFFF. The dielectrophoretic force (F_{DEP}) acting on the particles is several orders larger than the electrophoretic (F_{EP}) and sedimentational (F_{SED}) forces. It periodically varies along the flow channel, with the strongest force at the edges of the electrode segments.

planar μ-EFFF; however, particles accumulate at the edges of the electrode segments when a PV is applied. Other researchers observed similar particle trapping in the microdevices with polynomial and castellated electrode arrays.[15]

The forces acting on the particles at 1 μm distance from the segmented electrode are calculated and depicted in Figure 6. They vary along the flow channel, with the strongest forces acting at the edges of the electrode segments. The dielectrophoretic force is several orders of magnitude larger than the other forces; therefore, the particle movement is governed by DEP for the segmented μ-EFFF instead of electrophoresis for the planar μ-EFFF.

Particles are trapped because they undergo a positive DEP. They are generally more polarized than the aqueous medium at a low frequency due to the ionic double layer on the particle surfaces. Positive DEP is more effective for nanoparticle trapping because a particle experiencing negative DEP migrates away from the segmented electrode, and hence, the dieletrophoretic force on this particle decreases. Electric-field-induced fluid flow reported in other literature[15] was not observed in our study because it depends on the aqueous medium and the electrode design used. The particle trapping diminishes after the PV is stopped.

Mechanism of Planar μ-EFFF. On the basis of the particle movement observed in our experiments, the mechanism of planar μ-EFFF operated with a PV is illustrated in Figure 7.

When a PV is applied to the device, negatively charged particles migrate toward the top electrode with the positive polarity due to the electrophoresis. This electrophoretic force counteracted by drag and diffusive forces determines the lateral location of charged particles. Once the lateral coordinate of the charged particle is decided, its axial flow velocity will be governed by the parabolic flow profile of the carrier fluid. Particles closer to the wall electrode flow slower and stay longer in the channel; particles at the center moves faster and exit earlier from the channel. By modulating the pulse cycle in the PV operation, charged particles, which originally migrated toward the positively charged electrode, move to the middle lamina region of high flow velocity as the polarity of electrode reverses.

A generalized model for the FFF with a cyclical field applied was postulated by Giddings.[13] Particles in a cyclical FFF device were assumed to experience only one dominant force, which

(15) Ramos, A.; Morgan, H.; Green, N. G.; Castellaneous, A. *J. Phys. D: Appl. Phys.* **1998**, *31*, 2338−2353.

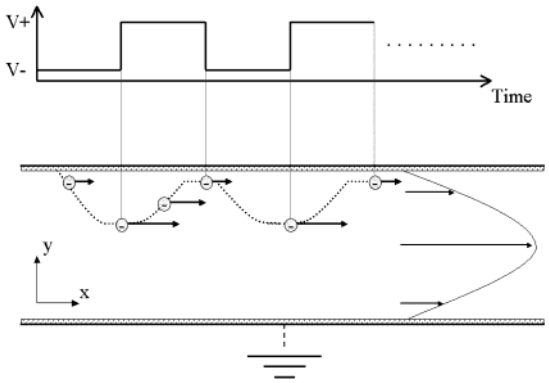

Figure 7. Schematic diagram of the mechanism for PV planar μ-EFFF. Charged particles inside the flow channel are driven toward or away from electrodes according to the polarity of the electrodes. As the polarity reverses every half cycle of the PV, the lateral migration of particle reverses, as well. As a result, particle velocity varies with time due to the changing locations of the particles in the carrier flow.

displaces the particles coherently with the cyclical field, that is, the electrophoretic force in EFFF. However, this assumption may fail to apply for the planar μ-EFFF operated with a PV. As the maximum potential applied to the device is limited by water electrolysis and a significant voltage is dissipated by electrode polarization, the applied potential only results in a weak effective electric field.[3,4,7] Because the particles in the channel simultaneously experience many other effects, such as sedimentation, Brownian motion, diffusion and DEP, the electrophoresis derived by the weak effective electric field may not be the governing effect. Especially for nanoparticles and small biomolecules, the effects of Brownian motion and diffusion become significant.

To our knowledge, this is the first study to postulate a model based on the in situ visualization experimental results that proves that electrophoresis is, indeed, the dominant effect on nanoparticle motion in a PV planar μ-EFFF.

Particle Trajectory for Segmented μ-EFFF. To examine the influence of PV, the motion of a single nanoparticle was visualized for the segmented μ-EFFF. (See Supporting Information on video Figure 8a.avi.) The particle movement was recorded at a carrier flow of 10 μL h^{-1} in absence of a PV at the beginning, then a PV was applied. The trajectory and velocity profile of the particle (Figure 8a and b, respectively) are extracted from the captured video by using a Matlab program. The velocity profile was analyzed to study the effect of the PV.

The particle is transported with an average carrier velocity along the flow channel at the beginning. Once a PV is applied, the particle migrates toward the segmented electrode and moves more slowly in axial direction due to the parabolic flow profile of the carrier fluid. The particle velocity reduces continuously down the channel.

Stable PV. The motion of a nanoparticle was recorded at a constant carrier flow after a PV had been applied to the system for a period of time. (See Supporting Information on video Figure 9.avi.)

Figure 9 shows the trajectory and velocity profile of the particle. The velocity profile can be divided into three significantly different regions: the electrode region (defined as the inner region of the conductive electrode), the gap region (defined as the inner region of the insulating gap), and the edge region (defined as the outer

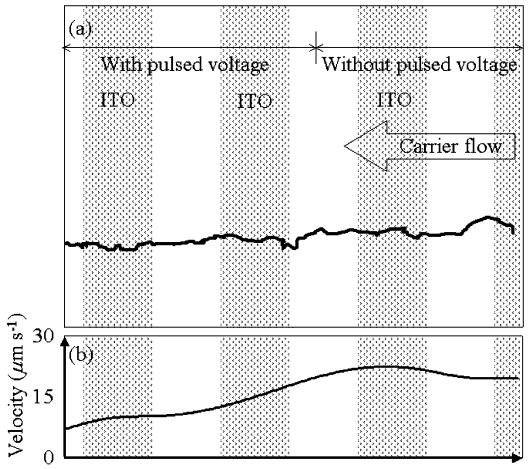

Figure 8. The effect of PV on (a) the trajectory and (b) the velocity of a single nanoparticle for the segmented μ-EFFF. The particle velocity reduces once a PV is applied as positive DEP directs the particle toward the segmented electrode. Carrier flow rate, 10 μL h^{-1}. PV operation is *off* before the experiment (image recording) starts.

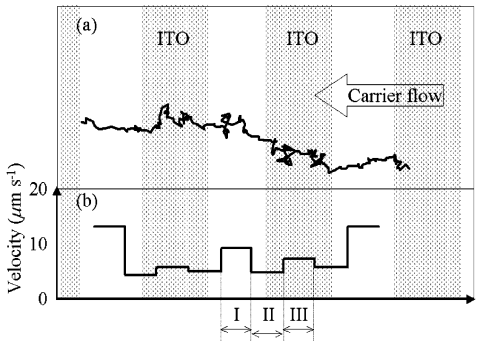

Figure 9. The trajectory and velocity profile of a single nanoparticle under a PV and a pressure-driven flow on the three different regions of a segmented μ-EFFF. Region I, inner insulating gap (15 μm in width); region II, edge of electrode and gap (15 μm in width); and region III, inner electrode (15 μm in width). The lowest velocity of the particle is found at the edge region because the particle is closer to the segmented electrode as a result of the strongest dielectrophoretic force acting on the particle. Carrier flow rate, 5 μL h^{-1}. PV operation is *on* before the experiment (image recording) starts.

region of both of the electrode and gap). All the three different regions defined above are 15 μm in width.

When the particle passes through the edge region, it experiences the strongest positive dielectrophoretic force. The particle is driven closer toward the segmented electrode, and therefore, its velocity decreases due to the parabolic profile of the carrier flow.

The influence of the diffusive force increases in the electrode region and, furthermore, in the gap region because the dielectrophoretic force in the gap region is the smallest. Hence, the particle moves closer to the middle of the channel, and its velocity increases.

Judging from the velocity profiles of the nanoparticle shown in Figures 8 and 9, it is clear that the particle velocity in Figure 8 does not vary among the gap, the edge, and the electrode regions as it does for Figure 9. This can be explained by the different PV conditions and carrier flow rates applied in these two case studies. For Figure 8, the effect of PV on the motion of a single nanoparticle was studied/recorded at a carrier flow rate of

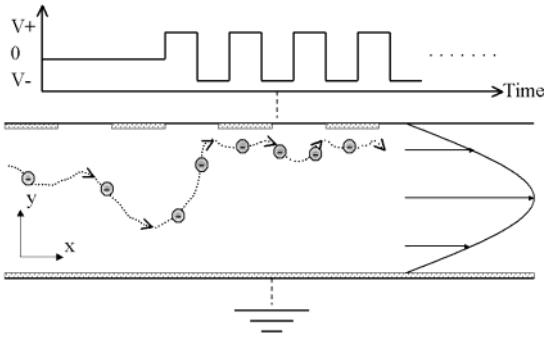

Figure 10. Schematic diagram of the mechanism for PV segmented μ-EFFF. Particle velocity is determined by particle lateral position in the carrier flow. The lateral position is governed by the dielectrophoretic and the diffusive forces acting on the particle. Because the dielectrophoretic force is spatially nonuniform, the particle velocity varies along the flow channel.

10 μL h^{-1}. Prior to the application of the PV, the nanoparticle can randomly position (i.e., in any lateral position) in the channel. As soon as the PV is turned on, the charged particle will gradually migrate toward the segmented electrode. The electric field effect of the segmented electrode (as simulated in Figure 4) is not significant in this experiment, because the charged nanoparticle may not be in the proximity of the segmented electrode. The small residence time of the particle because of a relatively high carrier flow rate may also help to explain the weak effect of dielectrophoresis in this case.

On the other hand, for the information shown in Figure 9, the nanoparticle motion in the segmented μ-EFFF was recorded at a carrier fluid rate of 5 μL h^{-1} *after* a PV had been applied to the device for a long period of time. Because the PV is turned on *before* the beginning of the experiment and a relatively small carrier flow rate is applied, the charged nanoparticle has a good chance to be in the neighborhood of the segmented electrode; therefore, the electric field or dielectrophoresis effect demonstrated in Figure 4 is much more significant in this scenario.

Mechanism of Segmented μ-EFFF. The mechanism of segmented μ-EFFF operated with a PV is illustrated in Figure 10. When the particles are injected into the channel in the absence of a PV, they spread over different heights of the flow channel and move with an average carrier velocity in the axial direction.

Once a PV is applied to the device, the particles experience a positive dielectrophoretic force and migrate toward the segmented electrode. Their accumulation creates a concentration gradient that causes the particles to diffuse away from the electrode. These two processes counteract on the particles and determine their lateral position in the carrier fluid, which influences the particle velocity. Because the dielectrophoretic force acting on the particles is spatially nonuniform because of a divergent electric field distribution in the flow channel, the particles levitate up and down; therefore the particle velocity varies along the flow channel. The slowest velocity is measured when the particles pass though the edges of the electrode segments due to the strongest dielectrophoretic force there.

Huang et al. discussed the principle of DEP-FFF using a device with an interdigitated electrode.[9,10] In their studies, the device was operated with a high-frequency AC excitation, and relatively large microparticles were used as samples. The lateral position of the particles was determined by assuming that only the force of gravitation and the average negative dielectrophoretic force influenced the position of the particles. The effects of Brownian motion and diffusion on the particles were ignored because they are insignificant for the relatively large microparticles.

However, Brownian motion and diffusion become significant for nanoparticles, whereas gravitation can be neglected. Therefore, in our case, which operated with a low frequency, the levitation of the nanoparticles is determined by the positive DEP and the diffusion instead of the gravitation and the negative DEP. Because the dielectrophoretic force on the particles varies along the flow channel, the levitation should be described by the momentary dielectrophoretic force acting on the particles instead of an averaged DEP. The hydrodynamic lifting effect can be neglected due to the low carrier flow rate used in our experiments.

CONCLUSION

To explore the potential of a PV μ-EFFF as a tool for sample separation in μ-TAS, experimental and theoretical investigations have been conducted. In this work, two μ-EFFFs with a top electrode of planar or segmented design were fabricated and characterized for nanoparticle movement under a PV. In comparison to the planar μ-EFFF, the electric field at the electrode segments of the segmented μ-EFFF is found to be stronger, with the strongest field at the edges of the electrode segments. In situ visualization experiments reveal that nanoparticle motion is governed by electrophoresis for planar μ-EFFF, whereas dielectrophoresis is the dominant effect imparted on the particles for segmented μ-EFFF. Two models are postulated to explain the particle movement under a PV. In contrast with the assumption that a particle travels with a fixed velocity due to a defined lateral particle position in the EFFF device operated with a constant voltage, the particle velocity varies along the flow channel under a PV due to a time-varied or spatially nonuniform driving force (i.e., electrophoretic or dielectrophoretic force) imparted on the particle. Therefore, the mean particle velocity should be expressed in an integral form.

Because a particle behaves differently in the PV μ-EFFF with respect to the electrode design of the device, the elution of the particle could be controlled by using different electrode designs.

ACKNOWLEDGMENT

This work was supported by grants from the Research Grants Council of Hong Kong SAR (HKUST 6019/02P, HKUST 6017/02E).

SUPPORTING INFORMATION AVAILABLE

Four videoclips showing the effect of PV on the motion of nanoparticle in absence of a carrier flow for planar μ-EFFF and segmented μ-EFFF, and the motion of a nanoparticle with a carrier flow under a transient PV and a stable PV for segmented μ-EFFF are available as Supporting Information. This material is available free of charge via the Internet at http://pubs.acs.org.

Received for review December 4, 2003. Accepted March 1, 2004.

AC035429Y